Journal of the Optical Society of America B
OPTICAL PHYSICS

Bandwidth control in 5 μm pulse generation by dual-chirped optical parametric amplification

Scott Wandel,[1,*] Ming-Wei Lin,[1] Yanchun Yin,[1] Guibao Xu,[1] and Igor Jovanovic[1,2]

[1]Department of Mechanical and Nuclear Engineering, Pennsylvania State University, University Park, Pennsylvania 16802, USA
[2]Department of Nuclear Engineering and Radiological Sciences, University of Michigan, Ann Arbor, Michigan 48109, USA
*Corresponding author: sfw5031@psu.edu

Received 24 March 2016; revised 8 June 2016; accepted 15 June 2016; posted 16 June 2016 (Doc. ID 261706); published 5 July 2016

We extend the technique of difference-frequency mixing of broadband chirped near-infrared (IR) pulses to longer wavelengths, thereby generating high-energy, bandwidth-tunable laser pulses in the mid-IR spectral region. Numerical modeling has been performed to examine the influence of pump and seed chirp on the generated idler bandwidth and pulse duration. The amplifier is realized using zinc-germanium phosphide crystals pumped by a 2 μm ultrafast parametric source. Idler pulses at a center wavelength of 5 μm with adjustable bandwidth are produced by equally chirping the pump and seed pulses using material dispersion. Using this simple approach, efficient generation of narrowband, short, mid-IR laser pulses is achieved without the use of high-loss dispersive gratings or prism pairs.

OCIS codes: (190.4410) Nonlinear optics, parametric processes; (190.4970) Parametric oscillators and amplifiers; (320.1590) Chirping; (320.5540) Pulse shaping.

http://dx.doi.org/10.1364/JOSAB.33.001580

1. INTRODUCTION

Significant developments of mid-infrared (IR) laser sources covering the spectral region from 2 to 25 μm have occurred over the last three decades due to their extensive application in areas such as laser spectroscopy [1] and strong-field physics [2]. In the mid-IR spectral region, organic and inorganic molecules show the strongest absorption features associated with fundamental vibrational resonances. Pump-probe spectroscopy of hydrogen-bonded molecular structures has been demonstrated by selective excitation of vibrational states within the mid-IR region [3]. Time-resolved IR Raman spectroscopy of polyatomic molecules in condensed phases has been shown using narrowband pump pulses and time-resolved absorbance probe pulses in the mid-IR [4]. High-energy, femtosecond-level mid-IR laser pulses have received considerable attention in many strong-field physics applications, including high-harmonic generation (HHG) [5] and laser-driven particle acceleration [6], as a result of the favorable ponderomotive energy scaling with the laser wavelength ($\propto \lambda^2$). Tunable, high-power mid-IR laser pulses are needed to simultaneously resolve the fast dephasing times and the narrow resonance dynamics of molecular vibrations and to effectively drive several innovative particles acceleration mechanisms.

In IR Raman spectroscopy, a tunable IR laser pulse irradiates a sample to a characteristic resonant vibrational excitation state, while an intense visible probe pulse is used to measure an incoherent anti-Stokes and Stokes Raman scattering spectrum. The intensity of the Raman scattering is directly proportional to the occupation of vibrational excited states. Excitation energies within the Raman spectrum vary as the sample is pumped to one excited state and subsequently decays to another. High-sensitivity transition measurements heavily rely on producing enough excited vibrations that can be detected above background levels. Mid-IR pulses are becoming increasingly popular over near-IR pulses for Raman spectroscopy with the emerging development of high-power mid-IR sources because absorption features of vibrations based on resonances in the near-IR are weaker harmonics of the strong fundamental resonances in the mid-IR. Complex molecular structures can have thousands of closely packed resonances; thus, tunable mid-IR sources are needed in Raman spectroscopy to selectively pump different excited states.

Particle accelerators with large acceleration gradients (> GV/m) are needed to supply relativistic beams on a small scale for high-energy physics experiments. Current metallic-resonator-based particle accelerators are limited to low drive powers because of structure breakdown. Dielectric structures with dimensions that scale with driving laser wavelength offer a solution to the problem of breakdown. Using a mid-IR laser source for dielectric laser acceleration greatly reduces multiphoton ionization leading to dielectric structure breakdown. Microfabricated dielectric laser accelerators (DLAs) are an attractive approach to the development of compact tabletop accelerators on the MeV-GeV scale. The so-called "accelerator on

a chip" technology based on spatial harmonics has been demonstrated recently using a laser wavelength of $\lambda = 800$ nm [7,8]. Operating with longer laser wavelengths relaxes the structure dimensions and permits larger structure apertures and stored energies, thereby allowing greater energies to be used to pump the structure. The corresponding accelerating field enhancement represents a potential reduction in the active accelerator length by 1–2 orders of magnitude. By leveraging the development of tunable, high-peak power mid-IR sources, laser-driven particle acceleration in dielectric photonics structures could enable high acceleration gradients (> GV/m), even at modest laser peak powers [6,9].

Although tunable mid-IR laser sources could benefit the performance of various optically driven applications, their production is technically challenging for a number of reasons. The mid-IR spectral region can be accessed through frequency downconversion of near-IR laser sources, such as Ti:sapphire or Nd:YAG, frequency upconversion of far-IR laser sources, such as CO_2 lasers, or directly by solid-state and fiber lasers that lase in the mid-IR, such as Ho:YAG [10,11]. A 1 GW Cr:ZnSe laser system has been developed that produces mid-IR 0.3 mJ laser pulses centered near 2.5 μm [12]. However, under high pump irradiances, Cr:ZnSe experiences strong thermal lensing leading to optical damage, significantly restricting its scalability to high average power. Tm-doped fiber lasers have achieved kW-level average powers in cw-operation [13]; however, pulsed Tm-fiber development has been limited due to the relatively low energy than can be stored within the fiber core without inducing detrimental $\chi^{(3)}$ nonlinearities. Recently, a Ho:YLF fiber laser was used to pump a zinc germanium phosphide (ZGP) optical parametric chirped-pulse amplification (OPCPA) to generate 7 μm laser pulses at a repetition rate of 100 MHz [14]; however, the energy scaling of the OPCPA is limited due to low-threshold thermal damage in the fiber pump laser. Even though CO_2 lasers are some of the most efficient lasers available, bandwidth limitations of the CO_2 medium have prevented production of subpicosecond mid-IR pulses by frequency upconversion. In addition, most current applications have preference for solid-state media. For these reasons, frequency downconversion from a high-power near-IR laser in a suitable nonlinear crystal represents the most viable approach to generating tunable, bandwidth-limited mid-IR laser pulses.

In this paper, we describe the development and performance of a mid-IR laser system capable of delivering short (femtosecond to picosecond) mid-IR laser pulses via optical parametric amplification (OPA) and examine the effect of pump and seed chirp on the generated idler spectral bandwidth through numerical modeling and experimentation. A two-stage optical parametric generator (OPG)/OPA design based on ZGP crystals pumped in the mid-IR spectral region [15] has been modified to produce bandwidth-tunable femtosecond laser pulses near 5 μm with μJ-level pulse energies and high shot-to-shot energy stability. The temporal profile of these mid-IR pulses is fully characterized using cross correlation that employs a standard silicon-based charge-coupled device (CCD). The source takes advantage of the optical characteristics of the nonlinear crystal ZGP for future direct mid-IR pumping and uses readily available bulk materials to generate sufficient chirp for bandwidth control, eliminating the need for complex and/or lossy dispersive gratings or chirped mirrors.

2. THEORY

Several approaches to generating tunable narrow-bandwidth laser pulses have been explored to date [16–23]. Linear spectral compression techniques include spectral filtering of broadband pulses with bandpass filters and inserting slits into the Fourier plane of a $4f$ pulse shaper. Nonlinear techniques to narrow-bandwidth pulse generation include self-phase modulation (SPM) in an optical fiber [16] and frequency conversion of chirped pulses in nonlinear gain media. One demonstrated technique uses counter-chirped pump and seed pulses in a potassium dihydrogen phosphate (KDP) crystal for sum-frequency generation [17]. Another approach uses equally chirped pump and seed pulses in a β-barium borate (BBO) crystal phase matched for difference-frequency generation (DFG) [18]. For applications requiring higher pulse energies (of order μJ to mJ) at longer wavelengths, such as HHG and DLA, OPA and OPCPA are desirable. A two-stage OPA based on BBO has been developed for narrowband picosecond pulse production using a spectrally filtered femtosecond pulse from the first amplification stage to seed the second amplification stage [19]. Many of the proposed and demonstrated approaches suffer from low efficiency, high complexity, limited spectral coverage, and difficulty in scaling to higher energies. Linear spectral filtering techniques based on absorption are relatively inefficient because the energy loss is proportional to the level of spectral narrowing. SPM in an optical fiber is limited to low pulse energies and small spectral compression ratios. Nonlinear methods, specifically frequency conversion of chirped seed and pump pulses, is an efficient technique for production of narrowband picosecond laser pulses from broadband femtosecond pulses. In DFG (and accordingly, OPA), the chirp of the generated idler pulse is equal to the difference between the chirps of the pump and seed pulses. The pump and seed pass through dispersive media to modulate their frequencies, given as $\omega_{ps}(t) = \omega_{p0,s0} + \beta_{p,s}t$, where ω_0 is the central frequency and β is the chirp (subscripts p and s refer to the pump and seed, respectively). The dispersive media stretch the pulses in time by a duration $\tau_{p,s} = \Delta\omega_{p0,s0}/\beta_{p,s}$, where $\Delta\omega$ is the spectral bandwidth. When pump and seed pulses linearly chirped with equal sign of temporal chirp mix in an OPA, the chirp of the generated idler pulse is reduced and can be eliminated for $\beta_p = \beta_s$:

$$\omega_i(t) = \omega_p(t) - \omega_s(t) = \omega_{p0} - \omega_{s0} + (\beta_p - \beta_s)t. \quad (1)$$

For the spectral narrowing effect to be realized, either positive or negative temporal chirp can be used, as long as it has the same sign for the pump and seed pulses. The maximum achievable spectral compression ratio of an OPA is limited not only by the magnitude of chirp imparted onto the pump and seed pulses but also by group velocity mismatch (GVM) between the pump and seed wavelengths. High GVM implies a narrow phase-matching bandwidth for the OPA process, effectively acting as a frequency filter that only amplifies spectral components of the pump and seed that are overlapped in time. In the case of chirped pulses, phase matching can be achieved for the pump, signal, and idler center wavelengths by introducing a time delay

δt on the pump, thereby shifting the frequency components of the pump by $\beta_p \delta t$. The addition of pump/seed chirp also increases the effective interaction length of the OPA stage, thus supporting the use of longer nonlinear crystals in the presence of high GVM.

Using this production technique for frequency doubling of chirped pulses is especially effective for narrow-bandwidth pulse generation because the two pulses are of the same frequency and have no GVM. This facilitates the use of longer crystals that can be used for highly efficient energy conversion without adversely affecting the generated pulse bandwidth [17]. Chirp-free pulse generation by frequency mixing chirped pump and seed pulses in the near-IR region (<2 μm) has been demonstrated in KDP [17], potassium titanyle arsenate (KTA) [20], and BBO [21]. This was possible in part by the availability of high-energy near-IR pump lasers and high-performance nonlinear crystals operating in this part of the spectrum. As mid-IR pump sources emerge with higher pulse energies and shorter pulse durations, this technique can be applied to generating narrow-bandwidth laser pulses at longer wavelengths using a new class of nonlinear crystals that require pumping in the mid-IR region, such as ZGP, silver thiogallate (AGS), or gallium selenide.

Mid-IR pumping presents a unique set of limitations on the system design because the dispersive materials suitable for this part of the spectrum are not as readily available as those in the near-IR region. Group-velocity dispersion (GVD) is typically introduced into systems by means of diffraction gratings, prism pairs, chirped mirrors, or bulk materials. Grating pairs are commonly used to control dispersion because they can generate more GVD than the other dispersive devices. Unfortunately, gratings often experience high losses due to higher-order diffraction and absorption in the metallic coatings of the gratings. Prism pairs can be highly efficient with appropriate antireflection coatings or with a near-Brewster's-angle arrangement; however, imperfect alignment can introduce multiple spatiotemporal distortions, including pulse-front tilt, spatial chirp, and angular dispersion. Gratings and prism pairs both require alternative dispersive elements to compensate higher-order dispersion terms. A grism-pair stretcher/compressor system may be used to simultaneously compensate second- and third-order dispersion (TOD) in chirped pulse amplifications [24]; however, grisms are typically inefficient and bulky. Chirped mirrors play a critical role in the generation of single-cycle pulses [25] because of their high reflectivity (>99%) and their ability to precisely control GVD and TOD using a small amount of material. However, due to interference between the reflections from different layers of a multilayer structure, GVD from chirped mirrors tends to be modulated across the spectrum. The magnitude of dispersion generated from chirped mirrors is also limited because of the relatively small difference in path length for a thin dielectric stack deposited on top of a substrate.

Previously demonstrated schemes for generation of narrowband pulses have differed in terms of the type of dispersive device used, spectral coverage, type of nonlinear crystal, and pulse energy range. For example, Veitas and Danielius demonstrated spectral narrowing in BBO [21] and KTA [20] using grating pairs. In BBO, 150 μJ pulses tunable in the range of 1025–1055 nm were produced with a compression ratio of ∼8. In KTA, 48 μJ at 3 μm and 5 μJ at 5 μm were produced with a compression ratio of ∼5. The longer-wavelength mid-IR pulses are more desirable for probing the strong fundamental vibrational resonances in molecular structures, but the long pulse duration (10 ps) of the generated pulses in KTA may be too long to resolve the fast dephasing times of stretching modes in certain molecules. Raoult *et al.* achieved a compression ratio greater than 30 in a KDP crystal around 529 nm using a grating pair [17], and Luo *et al.* achieved a compression ratio of ∼160 in a BBO crystal with a tuning range from 1000 to 1090 nm, also using a grating pair [18], but the limited spectral coverage severely restricts their use in applications requiring mid-IR radiation. More recently, Koller *et al.* used silicon prisms to generate narrow-bandwidth laser pulses tunable from 3.5 to 10 μm in an AGS crystal, but the total conversion efficiency was low (∼2%) due to a 65% loss in transmission across the entire prism pair setup [22]. The demonstrated approaches are inherently complex and lossy, involving the use of expensive and bulky dispersive mechanisms that are difficult to align and can generate spatial chirp.

Using bulk materials is an effective approach to generating dispersion in pump and seed pulses with a simple design that has no effect on the overall system footprint. The combined use of the appropriate lengths of materials with positive and negative GVD can generate tunable chirp on the mid-IR pulses. Bulk material selection for dispersion control depends on a number of different factors, including magnitude and sign of GVD and TOD, transmission, nonlinear absorption, and cost. We desire high GVD and transparency and low TOD and nonlinear absorption near 2 μm and 3.5 μm. TOD limits the applicability of using mixed dispersion materials of opposite sign of GVD because TOD is positive for all materials and cannot be eliminated by use of material dispersion alone. Materials with a low index of refraction at the pump and seed wavelengths are preferred to minimize losses arising from Fresnel reflections at normal incidence. It is advantageous to use a short length of material when generating dispersion to limit the accumulated parasitic effects, including higher-order dispersion, optical absorption, diffraction, self-focusing, and self-phase modulation.

At a given beam diameter, the most important consideration for material selection is providing sufficient dispersion without inducing significant nonlinear effects. To the first order, group delay dispersion (GDD) scales as $k''L$ and B integral as $n_2 L$, where k'' is the GVD, L is the material length, and n_2 is the nonlinear refractive index. To characterize dispersion management and compare different optical materials, it is useful to define the following figure of merit (FOM):

$$\mathrm{FOM} = k''/n_2. \tag{2}$$

The FOMs of several widely used materials in the mid-IR are displayed in Fig. 1. Laser pulses propagating dispersive materials experience diffraction over long lengths, so materials with a low refractive index are more attractive for maintaining small beam divergence. Germanium and silicon are highly dispersive at the pump and signal wavelengths but have low transmission and high refractive indices near 2 μm. Calcium fluoride and magnesium fluoride are highly transparent in the range of 1–7 μm but are not highly dispersive. Zinc selenide has small TOD within the mid-IR but also has small GVD at the pump

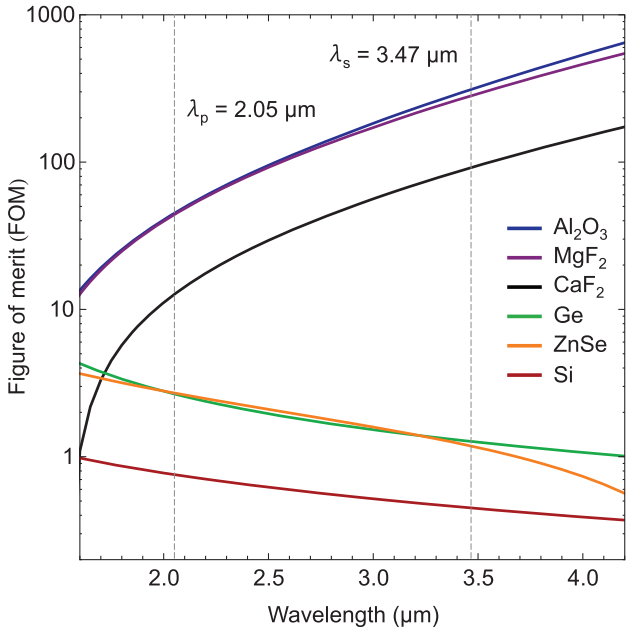

Fig. 1. Calculated FOM of sapphire (Al_2O_3), magnesium fluoride (MgF_2), calcium fluoride (CaF_2), germanium (Ge), zinc selenide (ZnSe), and silicon (Si) in the mid-IR spectral region near the pump (2.05 μm) and seed (3.47 μm) wavelengths.

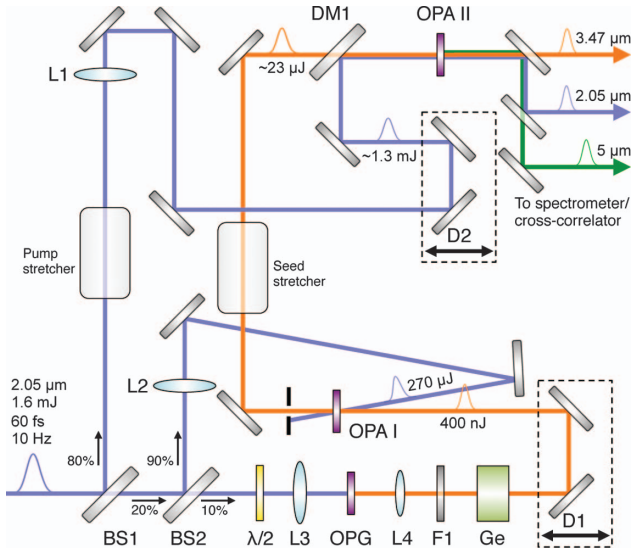

Fig. 2. Experimental setup of the dual-chirped OPA. Blue, 2.05 μm pump beam; orange, 3.47 μm signal (seed) beam; green, 5 μm idler beam. BS, beamsplitter; F, long-pass filter; DM, dichroic mirror; OPG, 1 mm thick ZGP crystal; OPA I, 1 mm thick ZGP crystal; OPA II, 1.5 mm thick ZGP crystal.

and signal wavelengths. Sapphire is a promising candidate material because of its low refractive index and relatively high GVD paired with excellent transmission below ~5 μm.

Due to its favorable group-velocity dispersion and excellent transparency in the mid-IR wavelength region, sapphire (Al_2O_3) was chosen as the primary material for stretching the pump and seed pulses in our experiment. The GVD in sapphire is −135 fs^2/mm and −935 fs^2/mm for the pump (2.05 μm) and signal (3.47 μm) wavelengths, respectively [26]. The transmission of sapphire is nearly uniform (~90%) in the range of 1–5 μm. The only modification to the source after inserting a sapphire window is an adjustment of the pump-seed delay.

3. SOURCE ARCHITECTURE

A schematic of our 5 μm OPA is presented in Fig. 2. The system is pumped with a 2 μm OPA, which itself is pumped by a Ti:sapphire chirped-pulse amplification system delivering 14 mJ, 40 fs laser pulses centered at 800 nm with a FWHM bandwidth of 25 nm at a repetition rate of 10 Hz. The 2 μm OPA system uses a two-stage mixed phase-matching scheme based on BBO crystals to produce mid-IR pulses with a pulse energy of 2.2 mJ and a pulse duration of 42 fs [27]. Previous work on 5 μm pulse production has shown that the use of a 60 fs pump pulse at 2 μm generates higher pulse energy with better conversion efficiency due to an increased pulse-splitting length in the second OPA stage [28]. The 5 μm parametric source uses two ZGP crystals with dimensions of 10 × 10 × 1.0 mm^3 and 10 × 10 × 1.5 mm^3 in the first and second OPA stage, respectively. Each crystal is cut at an angle of $\theta_m = 56.1^\circ$ for type I ($e_p \rightarrow o_s + o_i$) phase matching with a corresponding effective nonlinearity of 77.3 pm V^{-1}. Both OPA crystals are coated for all three wavelengths present in the OPA process. The majority of the pump pulse energy at 2 μm is reflected from BS1 and directed to the second OPA stage. The transmitted energy is subsequently split again, with a majority of the remaining energy reflected from BS2 and directed to the first OPA stage. The pulse energy transmitted by BS2 passes through a half-wave plate to rotate the polarization and an iris diaphragm to block the backreflection from the OPG crystal. The pump pulse with an energy of 25 μJ is focused onto a 1 mm thick ZGP crystal cut at an angle of $\theta_m = 56.1^\circ$ to produce an OPG signal centered at 3.47 μm. Although damage threshold measurements for femtosecond pulses in the mid-IR region are currently unavailable, we begin to observe slight surface damage when pumping the OPG crystal with a pulse intensity of 40 GW cm^{-2}. The OPG signal is collimated before passing through a 5 mm thick germanium stretcher with dispersion of 1277 fs^2 mm^{-1} at 3.47 μm, enabling selective amplification of different portions of the spectrum in the first OPA by adjusting the seed-pump delay. The residual pump beam energy is removed from the OPG signal pulse with a 1 mm thick long-wave-pass filter (LP-3000 nm, Spectrogon). In the first OPA crystal, the stretched OPG seed pulse with an energy of 400 nJ mixes with the pump pulse with an energy of 270 μJ at an angle of 4.6° to generate preamplified signal pulses at 3.47 μm with a pulse energy of 23 μJ. Dispersive material is placed in the pump beam path directly after being reflected from BS1 and in the seed beam path directly after the first OPA. A scanning delay line inserted in the pump beam path is used to match the timing of the pump and seed beams after being dispersed for mixing in the second OPA crystal. The 2.05 μm pump and 3.47 μm seed generate a 5 μm idler in the second OPA using an interaction angle of 2.1° to reduce the GVM effects and achieve a broad gain bandwidth.

4. NUMERICAL MODELING OF DUAL-CHIRPED OPTICAL PARAMETRIC AMPLIFICATION

A 1D numerical model for dual-chirped OPA is used to simulate three-wave parametric interaction in ZGP. In this study, the following assumptions and simplifications are made: (1) the gain medium is lossless, (2) interaction is collinear, (3) no diffraction is present (beams are plane waves), and (4) waves exist in a single spatial mode but are longitudinally multimode [29]. The coupled wave equations for three-wave mixing in a lossless medium assuming the slowly varying amplitude approximation ($|d^2A/dz^2| \ll |kdA/dz|$) can be written as [30]

$$\frac{dA_i(z)}{dz} = i\frac{2d_{\text{eff}}\omega_i^2}{k_i c^2}A_s^*(z)A_p(z)\ \exp(i\Delta kz), \tag{3}$$

$$\frac{dA_s(z)}{dz} = i\frac{2d_{\text{eff}}\omega_s^2}{k_s c^2}A_i^*(z)A_p(z)\ \exp(i\Delta kz), \tag{4}$$

$$\frac{dA_p(z)}{dz} = i\frac{2d_{\text{eff}}\omega_p^2}{k_p c^2}A_i(z)A_s(z)\ \exp(i\Delta kz), \tag{5}$$

with initial conditions $A_{i,s,p}(0) = |A_{i,s,p}(0)|\exp(i\phi_{i,s,p}(0))$. $A_{i,s,p}$ are the complex field amplitudes of the idler, signal, and pump wave, respectively, d_{eff} is the effective nonlinearity, $\omega_{i,s,p}$ is the angular frequency, $k_{i,s,p}$ is the wave vector, $\Delta k = k_p - k_s - k_i$ is the wave vector mismatch, c is the speed of light in vacuum, and $\phi_{i,s,p}(0)$ is the initial phase. The longitudinal coordinate is denoted by z. To address the important temporal characteristics of this process, the complex amplitude of the idler, signal, and pump pulses $A_{i,s,p}$ are represented in the time and frequency domain: $A_{i,s,p} = A_{i,s,p}(t) = \mathcal{F}^{-1}[A_{i,s,p}(\omega)]$, including the corresponding amplitude and phase.

While the nonlinear mixing process is described in the time domain, dispersion is more readily represented in the spectral domain. Dispersion is included in the model using the usual split-step approach [31], by transforming the fields into the spectral domain after each step of numerical integration in the time domain. The spectral phase applied to the three fields at each step is

$$A_{i,s,p}(\omega) \rightarrow A_{i,s,p}(\omega)\ \exp(in_{i,s,p}(\omega)\omega/c), \tag{6}$$

where ω is the angular frequency and $n(\omega)$ is the refractive index for the corresponding spectral component ω of $A_{i,s,p}$. The incident idler, seed (signal), and pump beams are centered at 5 μm, 3.47 μm, and 2.05 μm, respectively. The incident seed and pump pulses are assumed to have a Gaussian spectral profile with a spectral bandwidth chosen such that their initial transform-limited pulse duration is 100 fs. Phase matching is achieved by orienting the ZGP crystal at 56.1° with respect to its principal axis.

Figure 3(a) shows the measured pump and preamplified signal pulses used for mixing in the dual-chirped OPA stage. The calculated idler spectra produced using our numerical model with varying pump and seed GDD is presented in Fig. 3(b), with the chirp parameters listed in Table 1. For comparison, the case of unchirped pump and seed pulses is also shown. As the magnitude of GDD increases, the idler bandwidth narrows. This is evident in the second-order nonlinear interaction term:

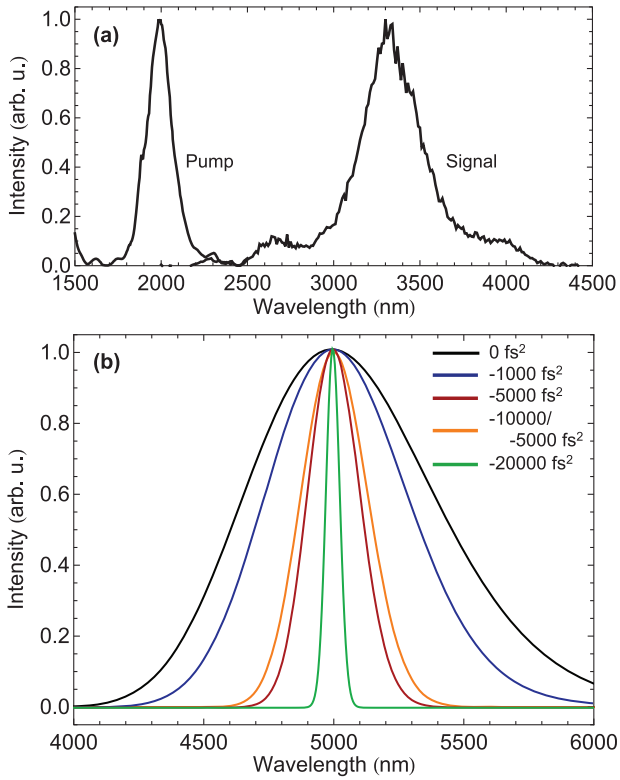

Fig. 3. (a) Measured pump and signal spectra used for dual-chirped OPA and (b) calculated idler spectra from ZGP OPA using equally chirped input pump and seed pulses varying in magnitude as described in Table 1.

Table 1. Model Parameters for Pump and Seed

	GDD_p (fs^2)	GDD_s (fs^2)	$\Delta\lambda$ (nm)	$\Delta\tau$ (fs)
1.	0	0	774	47
2.	−1000	−1000	601	61
3.	−10000	−5000	251	214
4.	−5000	−5000	187	196
5.	−20000	−20000	46	798

$$A_p\ \exp(i\omega_p t)[A_s\ \exp(i\omega_s t)]^* = \exp[-(\alpha_p + \alpha_s)t^2]\exp[i(\omega_p - \omega_s)t + i(\beta_p - \beta_s)t^2], \tag{7}$$

where $\alpha_{p,s} = 2\ \ln\ 2/\Delta t_{p,s}^2$ and $\Delta t_{p,s}$ represents the pulse duration of the pump and seed. The first exponential term on the right-hand side of the equation stands for the idler pulse envelope and the second exponential term originates from frequency mixing. The linear chirp of the idler pulse vanishes when the pump and seed pulses are chirped with the same value of GDD. The envelope, $\exp[-(\alpha_p + \alpha_s)t^2]$, has long pulse duration independent of the sign of chirp, and we expect to obtain narrow-bandwidth, chirp-free pulses when mixing pump and seed pulses with the same value of GDD. When the pump and seed chirp are not matched, the generated idler has residual chirp and departs from transform-limited pulse duration.

5. EXPERIMENTAL RESULTS AND DISCUSSION

We use a 10 cm long sapphire rod and a 15 mm thick sapphire window to chirp the 2.05 μm pump and the 3.47 μm seed, respectively. Using a pump pulse intensity of 11 GW cm^{-2}, the calculated B integral for propagation in the sapphire rod is 0.87. No noticeable self-focusing effects were observed in the beam profile, but upon further investigation, the pump beam experienced spectral broadening due to SPM. SPM leads to spectral broadening if the pulse is initially unchirped or positively chirped and narrowing if the pulse is initially negatively chirped. It has already been determined that the pump pulses are slightly positively chirped after performing phase retrieval measurements with second-harmonic generation frequency-resolved optical gating [27]. SPM was suppressed by reducing the pump pulse energy to 1.3 mJ. The measured pump pulse spectra for different pulse energy attenuation factors are shown in Fig. 4. When full energy (100%) is used, the spectral bandwidth of pump pulses increases by a factor of 2 after propagation through the sapphire rod. The spectral bandwidths before and after the rod are closely matched when ≲80% of the available pulse energy is used. At this reduced pulse energy, the B integral is calculated to be 0.7. The loss in transmission through the sapphire rod is ∼20% of the incident energy; 14% of the losses arise from Fresnel reflections, as calculated using a refractive index of $n = 1.737$ [26]. The remaining losses are mainly due to optical absorption in sapphire.

Stretching the pump pulse duration improves the conversion efficiency of the OPA stage because it increases the pulse-splitting length, defined as the effective interaction length over which pulses remain temporally overlapped within the crystal. Because ZGP has relatively large GVM for the three interacting waves, the pulse-splitting length for a 60 fs pump pulse is only 0.42 mm. A 10 cm sapphire rod stretches the pump pulse duration to ∼890 fs (assuming a transform-limited Gaussian pulse duration of 42 fs). At this pulse duration, GVM effects can be neglected because the crystal length being used (1.5 mm) is shorter than the pulse-splitting length (6 mm).

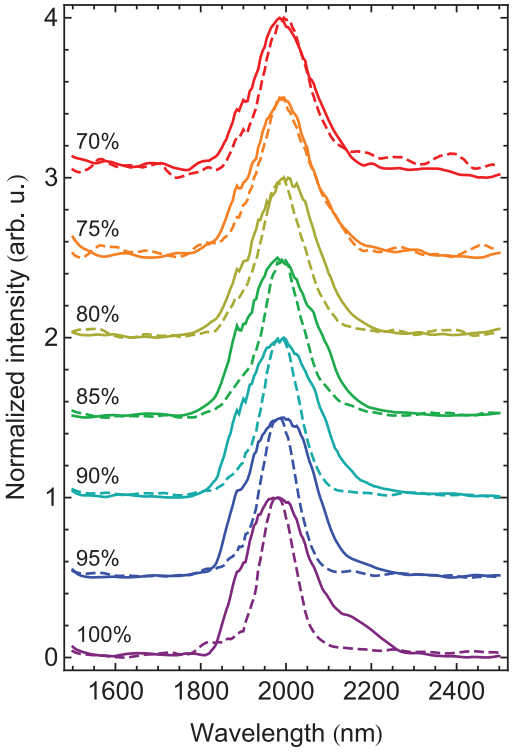

Fig. 4. Measured pump pulse spectra before (dashed) and after (solid) propagating a 10 cm thick sapphire rod with varying pulse intensities. For high pump intensities, large SPM leads to spectral broadening.

The spectrum of amplified pulses was measured using a 0.55 m monochromator (300 mm^{-1} grating blazed at 4 μm) in combination with a thermoelectrically cooled InSb photodetector. The monochromator has a detection range of 1–6 μm. Temporal profile of amplified idler pulses is measured by DFG cross correlation with a portion of the unconverted 800 nm pump from the 2 μm OPA system. Pulses of 800 nm have been fully characterized previously by spectral interferometry for direct E-field reconstruction. The idler output from the ZGP OPA system and the 800 nm reference pulse combine on a dichroic mirror and mix collinearly in a 1 mm thick MgO:LiNbO$_3$ crystal cut at an angle of $\theta_m = 46.2°$. Production of the cross-correlated DFG signal allows for indirect measurement of 5 μm idler pulses using a standard silicon-based CCD photodetector. The cross-correlation signal wavelength (952 nm) is sufficiently separated from the pump wavelength to allow spectral filtering to remove residual pump energy after the mixing process. A delay line was used to scan the temporal overlap of the two beams to obtain a cross-correlation trace.

Experimental results are in good agreement with results from the numerical model presented in Section 3. The idler bandwidth and pulse duration were both measured and calculated for a series of different pump and seed GDD values, as shown in Fig. 5. Figure 5(a) represents the case in which no additional dispersive materials have been added to the beam path. The original spectral bandwidth (prior to narrowing) is equal to 730 nm with a pulse duration of 700 fs, corresponding to a time-bandwidth product of 6.13. The measured spectral bandwidth supports a transform-limited pulse duration of 50 fs (approximately three optical cycles). Without dispersion management, the idler pulse experiences a large accumulation of GDD due to the presence of focusing optics, dielectric filters, and pulse stretcher in the pump and seed beam paths. Figure 5(b) represents the case in which the GDD imparted on the pump and seed pulses is −3500 fs^2. This magnitude of dispersion in achieved in the experiment by adding a combination of CaF_2 and sapphire windows to the beam path. The generated idler spectrum is narrowed to 440 nm, with a pulse duration of 370 fs, corresponding to a time-bandwidth product of 1.95. In the last case, represented in Fig. 5(c), the GDD of the pump and the seed pulses is −12000 fs^2. This is achieved by adding a 10 cm long sapphire rod to the pump beam and a 15 mm thick sapphire window to the seed beam. For this case, the generated idler pulse spectrum is compressed further to a bandwidth of 130 nm, with a pulse duration of 970 fs, corresponding to a time-bandwidth product of 1.51. In all three cases, the measured pulse spectrum matches well with the calculated pulse spectrum. On the other hand, the measured pulse durations do not match the calculated transform limited pulse

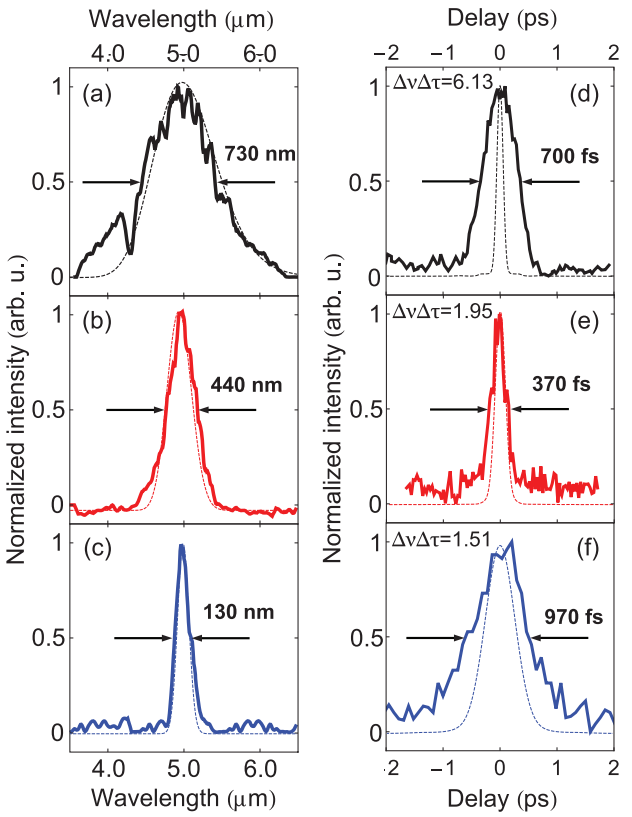

Fig. 5. Amplified idler pulse spectra and cross correlations at 5 μm for (a) and (d) no additional chirping mechanisms, (b) and (e) GDD = −3500 fs^2 for pump and seed, and (c) and (f) GDD = −12000 fs^2 for pump and seed. Solid, measured results; dashed, calculated pulse spectra (a)–(c) and calculated transform-limited pulse durations (d) and (e).

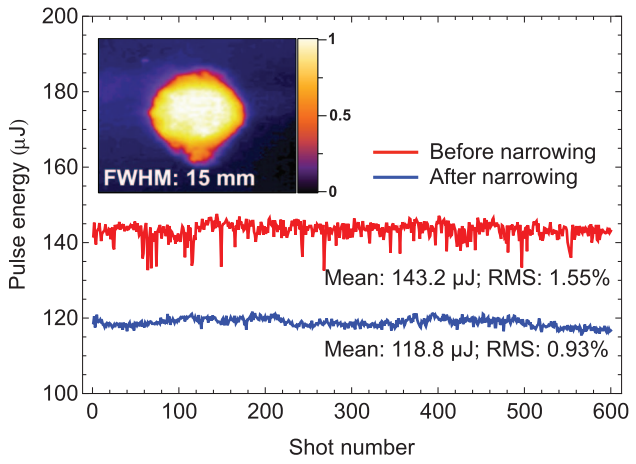

Fig. 6. Amplified signal + idler pulse energy before (red) and after (blue) adding dispersive material for spectral narrowing; inset, far-field beam profile measured with InSb array camera.

durations. In the first case, this can be attributed to a lack of dispersion compensation following amplification. In the last two cases, where dispersion is added to equally chirp the pump and seed pulses prior to mixing in the OPA, the measured pulse duration is much closer to the calculated transform-limited pulse duration. The deviation from transform-limited pulses can be attributed to higher-order dispersion terms that cannot be compensated using material dispersion and imperfect chirp matching of the pump and seed. In principle, the generated idler pulses are compressible by accurate dispersion management after the amplification stage to achieve near-transform-limited pulse durations.

The described source architecture produces laser pulses with excellent shot-to-shot energy stability and a uniform beam profile, as shown in Fig. 6. Energy measurements were performed using a pyroelectric detector, providing a sensitivity of ∼20 nJ, in combination with a LP-2500 nm filter to block unconverted pump energy. Without introducing additional dispersive materials for bandwidth narrowing, the laser system produces a combined signal + idler energy of 143 μJ after the second OPA stage, representing a 7.5% conversion efficiency from the total pump energy. After we insert an appropriate amount of material to generate a GDD of −12000 fs^2 onto the pump and seed pulses, the second OPA produces a total signal + idler pulse energy of 119 μJ after the second OPA, which represents a 14% conversion efficiency. The generated signal + idler energy is lower after adding dispersive material because the pump energy is reduced due to material reflection and absorption. Nevertheless, the conversion efficiency of the OPA is nearly 2 times larger in the design using bulk materials for bandwidth reduction, mostly because the pulse-splitting length of the OPA crystal is increased due to temporal broadening that accompanies dispersion.

6. CONCLUSION

We have presented a double-chirped parametric source design that is capable of producing femtosecond mid-IR pulses with tunable bandwidth. Greater than fivefold bandwidth reduction has been demonstrated experimentally. The system employs optical parametric amplification in a ZGP crystal to produce the mid-IR output at 5 μm using a high-energy 2 μm OPA as the pump source. The source is seeded with OPG at a center wavelength of 3.47 μm produced in a ZGP crystal. Both the pump and seed beams are chirped with equal GDD prior to mixing in the second OPA stage to generate narrow-bandwidth idler pulses tunable from 730–130 nm.

Because of the SPM leading to spectral broadening within the sapphire rod used to add GDD to the pump beam, it was necessary to reduce the pump pulse energy. In the future, a telescope can be used to resize the pump beam incident on the sapphire rod, thereby allowing higher pump energies. Alternatively, we may choose to pump the system with a longer wavelength, using one of the emerging high-energy mid-IR laser sources, such as Cr:ZnSe, to operate closer to degeneracy and enable the use of shorter material length to generate requisite dispersion. Using a pump wavelength of 2.5 μm as opposed to 2.05 μm reduces the length of sapphire needed to generate the same magnitude of dispersion by a factor of 2. Reducing the length of bulk material used is beneficial not only for reducing the effect of optical absorption but also for producing transform-limited pulses. The latter is the case because of the difficulty of compensating the higher-order dispersion terms

using material dispersion alone. The demonstrated approach to spectral narrowing offers highly efficient energy conversion in comparison to spectral filtering in a simple and robust design that does not require the use of refractive or diffractive elements to introduce dispersion.

Production of bandwidth-tunable mid-IR pulses that are closer to the transform limit requires more sophisticated control of initial spectral phase. One way to achieve this is by the use of a programmable phase tuner, such as a liquid crystal pulse shaper, to further compensate higher-order dispersion terms. With the demonstrated spectral widths and pulse durations described herein, this parametric system is nevertheless attractive for applications including Raman spectroscopy and dielectric laser acceleration.

Funding. U.S. Department of Energy (DOE); Defense Advanced Research Projects Agency (DARPA) (N66001-11-1-4197).

REFERENCES

1. F. K. Tittel, D. Richter, and A. Fried, "Mid-infrared laser applications in spectroscopy," in *Solid-State Mid-Infrared Laser Sources*, I. T. Sorokina and K. L. Vodopyanov, eds. (Springer, 2003), pp. 445–516.
2. B. Wolter, M. G. Pullen, M. Baudisch, M. Sclafani, M. Hemmer, A. Senftleben, C. D. Schröter, J. Ullrich, R. Moshammer, and J. Biegert, "Strong-field physics with mid-IR fields," Phys. Rev. X **5**, 021034 (2015).
3. J. A. Gruetzmacher and N. F. Scherer, "Few-cycle mid-infrared pulse generation, characterization, and coherent propagation in optically dense media," Rev. Sci. Instrum. **73**, 2227–2236 (2002).
4. J. C. Deàk, L. K. Iwaki, and D. D. Dlott, "High-power picosecond mid-infrared optical parametric amplifier for infrared Raman spectroscopy," Opt. Lett. **22**, 1796–1798 (1997).
5. M.-C. Chen, C. Mancuso, C. Hernández-Garcia, F. Dollar, B. Galloway, D. Popmintchev, P.-C. Huang, B. Walker, L. Plaja, A. A. Jaroń-Becker, A. Becker, M. M. Murnane, H. C. Kapteyn, and T. Popmintchev, "Generation of bright isolated attosecond soft X-ray pulses driven by multicycle midinfrared lasers," Proc. Natl. Acad. Sci. USA **111**, E2361–E2367 (2014).
6. B. Naranjo, A. Valloni, S. Putterman, and J. B. Rosenzweig, "Stable charged-particle acceleration and focusing in a laser accelerator using spatial harmonics," Phys. Rev. Lett. **109**, 164803 (2012).
7. E. A. Peralta, K. Soong, R. J. England, E. R. Colby, Z. Wu, B. Montazeri, C. McGuinness, J. McNeur, K. J. Leedle, D. Walz, E. B. Sozer, B. Cowan, B. Schwartz, G. Travish, and R. L. Byer, "Demonstration of electron acceleration in a laser-driven dielectric microstructure," Nature **503**, 91–94 (2013).
8. J. Breuer and P. Hommelhoff, "Laser-based acceleration of nonrelativistic electrons at a dielectric structure," Phys. Rev. Lett. **111**, 134803 (2013).
9. J. Rosenzweig, A. Murokh, and C. Pelligrini, "A proposed dielectric-loaded resonant laser accelerator," Phys. Rev. Lett. **74**, 2467–2470 (1995).
10. T. Kanai, P. Malevich, S. Kangaparambil, H. Hoogland, R. Holzwarth, A. Pugzlys, and A. Baltuska, "110-fs, 5.3-μm ZGP parametric amplifier driven by a ps Ho:YAG chirped pulse amplifier," in *CLEO: Science and Innovations* (Optical Society of America, 2016), paper STu3I.2.
11. P. Krogen, H. Liang, K. T. Zawilski, P. G. Schunemann, T. Lang, U. Morgner, J. A. Moses, F. X. Kaertner, and K.-H. Hong, "Octave-spanning 1.5-optical-cycle 6.5-μm OPA pumped by 2.1-μm OPCPA," in *CLEO: Science and Innovations* (Optical Society of America, 2016), paper STu3I.4.
12. P. Moulton and E. Slobodchikov, "1-GW-peak-power, Cr:ZnSe laser," in *CLEO: Laser Applications to Photonic Applications*, OSA Technical Digest (Optical Society of America, 2011), paper PDPA10.
13. T. Ehrenreich, R. Leveille, I. Majid, K. Tankala, G. Rines, and P. Moulton, "1-kW, all-glass Tm:fiber laser," Proc. SPIE **16**, 7580 (2010).
14. D. Sanchez, M. Hemmer, M. Baudisch, S. Cousin, K. Zawilski, P. Schunemann, O. Chalus, C. Simon-Boisson, and J. Biegert, "7 μm, ultrafast, sub-millijoule-level mid-infrared optical parametric chirped pulse amplifier pumped at 2 μm," Optica **3**, 147–150 (2016).
15. S. Wandel, G. Xu, Y. Yin, and I. Jovanovic, "Parametric generation of energetic short mid-infrared pulses for dielectric laser acceleration," J. Phys. B **47**, 234016 (2014).
16. M. Oberthaler and R. A. Höpfel, "Special narrowing of ultrashort laser pulses by self-phase modulation in optical fibers," Appl. Phys. Lett. **63**, 1017 (1993).
17. F. Raoult, A. C. L. Boscheron, D. Husson, C. Sauteret, A. Modena, V. Malka, F. Dorchies, and A. Migus, "Efficient generation of narrow-bandwidth picosecond pulses by frequency doubling of femtosecond chirped pulses," Opt. Lett. **23**, 1117–1119 (1998).
18. H. Luo, L. Qian, P. Yuan, and H. Zhu, "Generation of tunable narrow-band pulses initiating from a femtosecond optical parametric amplifier," Opt. Express **14**, 10631–10635 (2006).
19. S. Shim and R. A. Mathies, "Generation of narrow-bandwidth picosecond visible pulses from broadband femtosecond pulses for femtosecond stimulated Raman," Appl. Phys. Lett. **89**, 121124 (2006).
20. G. Veitas, R. Danielius, and E. Schrieber, "Efficient generation of $< 3\ cm^{-1}$ bandwidth mid-IR pulses by difference-frequency mixing of chirped pulses," J. Opt. Soc. Am. B **19**, 1411–1418 (2002).
21. G. Veitas and R. Danielius, "Generation of narrow-bandwidth tunable picosecond pulses by difference-frequency mixing of stretched pulses," J. Opt. Soc. Am. B **16**, 1561–1565 (1999).
22. F. O. Koller, K. Haiser, M. Huber, T. E. Schrader, N. Regner, W. J. Schreier, and W. Zinth, "Generation of narrowband subpicosecond mid-infrared pulses via difference frequency mixing of chirped near-infrared pulses," Opt. Lett. **32**, 3339–3341 (2007).
23. M. Marangoni, D. Brida, M. Quintavalle, G. Cirmi, F. M. Pigozzo, C. Manzoni, F. Baronio, A. D. Capobiano, and G. Cerullo, "Narrow-bandwidth picosecond pulses by spectral compression of femtosecond pulses in a second-order nonlinear crystal," Opt. Express **15**, 8884–8891 (2007).
24. S. Kane and J. Squier, "Grism-pair stretcher–compressor system for simultaneous second- and third-order dispersion compensation in chirped-pulse amplification," J. Opt. Soc. Am. B **14**, 661–665 (1997).
25. V. Pervak, V. Tikhonravov, M. K. Trubetskov, S. Naumov, F. Krausz, and A. Apolonski, "1.5-octave chirped mirror for pulse compression down to sub-3 fs," Appl. Phys. B **87**, 5–12 (2007).
26. I. H. Malitson and M. J. Dodge, "Refractive index and birefringence of synthetic sapphire," J. Opt. Soc. Am. **62**, 1405 (1972).
27. G. Xu, S. Wandel, and I. Jovanovic, "Nondegenerate parametric generation of 2.2-mJ, few-cycle 2.05-μm pulses using a mixed phase matching scheme," Rev. Sci. Instrum. **85**, 023102 (2014).
28. S. Wandel, M.-W. Lin, Y. Yin, G. Xu, and I. Jovanovic, "Parametric generation and characterization of femtosecond mid-infrared pulses in $ZnGeP_2$," Opt. Express **24**, 5287–5299 (2016).
29. Y. C. Yin, D. French, and I. Jovanovic, "Ultrafast temporal pulse shaping via phase-sensitive three-wave mixing," Opt. Express **18**, 18471–18482 (2010).
30. Y. R. Shen, *The Principle of Nonlinear Optics* (Wiley, 2003).
31. M. D. Feit and J. A. Fleck, Jr., "Computation of mode properties in optical fiber waveguides by a propagating beam method," Appl. Opt. **19**, 1154–1164 (1980).